

## EFFECT OF Zn CONTENT ON CORROSION BEHAVIOR OF Mg-Y-Zn ALLOYS

Y. Shi <sup>a</sup>, X.-Q. Liu <sup>a,b,\*</sup>, Z.-L. Liu <sup>a,b</sup>, H.-J. Xie <sup>a</sup>, Y.-H. Wang <sup>a</sup>, J. Li <sup>b,c</sup>

<sup>a</sup> College of Materials Science and Technology, Nanjing University of Aeronautics and Astronautics, Nanjing, Jiangsu, China

<sup>b</sup> Jiangsu (Zhongyi) Engineering Research Center of Light Alloy Precision Die Casting, Changshu, Jiangsu, China

<sup>c</sup> Jiangsu Favour Automotive New Stuff Sci-Tech Co., Ltd., Changshu, China

(Received 25 May 2021; accepted 05 October 2021)

### Abstract

The microstructure, corrosion behavior, and electrochemical behavior of as-cast Mg-4Y-xZn ( $x=1,2,3,4$  wt.%) are studied by SEM, weight loss and electrochemical tests.  $Mg_{12}YZn$  ( $X$ ),  $Mg_3Y_2Zn_3$  ( $W$ ) and  $Mg_{24}Y_5$  constitute the phase composition system of the alloy. When Zn content is 1 wt.%, all tests reveal that alloy has the optimal corrosion performance. The second phase in these alloys, due to their nobler nature than  $\alpha$ -Mg, exists as a cathode during the corrosion process, so that  $\alpha$ -Mg preferentially occurs corrosion to accelerate the formation of corrosion pits. After soaking in 3.5 wt.% NaCl solution for some time, the stability of the  $W$  phase changed, and gradually dissolved, which was finally removed by chromic acid used for removal of corrosion products. In addition,  $X$  phase can be used as an anode in the micro-galvanic cells formed with  $W$  phase to reduce the corrosion rate of  $\alpha$ -Mg and thus improve the corrosion performance of the alloy.

**Keywords:** Mg-Y-Zn; Second phase; Corrosion behaviors; Electrochemical behaviors

### 1. Introduction

As the most promising lightweight and green engineering material, magnesium alloy has the advantages of light specific gravity, high specific strength, good damping performance, and easy recycling; making it has a wide range of application prospects in the electronic communications, aerospace, and other fields [1-5]. However, the development of magnesium alloy is hindered due to its low absolute strength and poor corrosion resistance [6, 7].

Recently, Mg-Y-Zn series alloys have aroused a lot of attention because of their excellent performance [8-13]. Furthermore, the effect of the LPSO structure on relative corrosion performance and how to enhance the corrosion resistance are currently being explored. Zhang et al. revealed corrosion pits were mostly concentrated at the junction of the LPSO phase and  $\alpha$ -Mg, which reflected that the LPSO phase accelerated the micro-galvanic corrosion of  $\alpha$ -Mg [14]. C. Q. Li et al. found that the LPSO with different volume fraction affected the corrosion performance of the alloy. The dense and thick LPSO phase hindered the corrosion expansion to a certain extent. The distribution of

LPSO phase changed the morphology of corrosion pits by affecting the shape of magnesium dendrite [15]. Lei Bao et al. also proposed that the species of the phase in the alloy affected the corrosion resistance and mechanism.  $W$  phase causes severe intergranular corrosion and forms micropores. Dense lath LPSO phase can effectively protect the matrix [16]. Similar results have been confirmed in many subsequent studies [17-22].

Based on the above research, it mainly covers the influence of LPSO phase content and morphology on the corrosion performance and process of magnesium alloy, while  $W$  phase is not conducive to the mechanical and corrosion properties of magnesium alloy. However, recent studies have shown that when LPSO and  $W$  phase coexist in the alloy, they have synergistic effect on the mechanical performance of the alloy [23]. At present, there are few researches on the corrosion properties of the magnesium alloy with the LPSO and  $W$  phase, so it is necessary to study its mechanism.

Therefore, based on the current research background, the relationship between the corrosion behavior of the phase and the  $\alpha$ -Mg needs to be further investigated. In this paper, Mg-4Y-xZn

\*Corresponding author: liuxiqin@nuaa.edu.cn



( $x=1,2,3$  and 4 wt.%) alloys with different second phases and their contents were studied with the aim of elucidating the relationship between the phases and the corrosion mechanism of the alloys.

## 2. Materials and methods

### 2.1. Alloys preparation and microstructural analysis

The studied alloys were manufactured by melting pure Mg, pure Zn and Mg-30% Y master alloys. Table 1 shows the chemical compositions of the studied alloys. The protective gas is a mixture atmosphere in which the volume ratio of SF<sub>6</sub> to CO<sub>2</sub> is 1:100. It was smelted in a steel crucible at about 720 °C, stirred at 740 °C for 30 min, and then cast in a preheated (~ 200 °C) iron mold at about 720 °C. The ingot size was 25×100×150 mm.

**Table 1.** The chemical compositions of the studied alloys

Alloys	Chemical compositions /wt.%		
	Y	Zn	Mg
WZ41	4	1	Balance
WZ42	4	2	Balance
WZ43	4	3	Balance
WZ44	4	4	Balance

The samples were mechanically grinded by SiC paper (from 120 grit to 3000 grit), then mechanically polished with 0.5 μm diamond paste. The X-ray diffractometer (XRD, MXP2NAHF) taking scanning range of 10°-90° with increments of 2θ and scanning rate of 5°/min with Cu Kα radiation at 40 kV and 150 mV which was used for phase identification of the samples and corrosion products. The microstructure, intermetallic compounds, and corrosion morphology of the specimens were observed by scanning electron microscopy (SEM, LYRA3TESCAN). The phase compositions were analyzed by the energy dispersive spectroscopy (EDS) equipped in SEM.

### 2.2. Immersion tests and mass loss tests

For the purpose of exploring the corrosion properties of different samples, the soaking experiment was taken in 3.5 wt.% NaCl solution at 25 °C for a certain time. Before immersion, the specimens were grinded by SiC papers down to 2000 grit. The ratio of the surface area of the specimen to the volume of NaCl solution was controlled at 1:100 (surface exposed to the solution was 6 cm<sup>2</sup> to 600 ml). After immersion, the sample was washed in a hot mixture of 200 g/L CrO<sub>3</sub>+10 g/L AgNO<sub>3</sub> to remove the corrosion products on the alloy, and then cleaned with distilled water and desiccated in the oven. Then,

the corrosion morphology of the corroded specimens was observed by SEM. The actual corrosion rate of the alloy is evaluated by the mass loss before and after the removal of corrosion products, and is calculated by the following formula:

$$CR = \frac{8.76 \times 10^4 \times \Delta g}{A \times t \times \rho} \quad (1)$$

Where  $\Delta g(g)$  is the mass loss,  $A(\text{cm}^2)$  is the surface area of the specimen,  $t(\text{h})$  is the soak time and  $\rho(\text{g/cm}^3)$  is the alloy density. Three experiments were carried out on the four alloys and the average values were applied.

### 2.3. Electrochemical tests

In 3.5 wt.% NaCl solution, the alloy was electrochemically tested by standard three electrode cell in Zahner Zennium electrochemical workstation. Among them, four specimens acted as working electrodes, a platinum electrode acted as the counter electrode, a saturated calomel electrode (SCE) acted as a reference electrode. All specimens were sealed with epoxy resin plastic, 1 cm<sup>2</sup> exposed surface was used as working electrode surface, and the other end was connected with copper wire. EIS measurement was taken in the frequency range of 100 kHz-10 mHz, using 10 mv sinusoidal voltage, and the experimental results were fitted by ZsimpWin. Potentiodynamic scanning was carried out at the rate of 1 mv/s, the limit of polarization current was -100 mA for the cathode and 100 mA for the anode. The above experiments were carried out after the samples were stabilized at open circuit potential (OCP) for 30 min.

## 3. Results and Discussion

### 3.1. Phase constitutions and microstructure observation

Fig. 1 shows the XRD spectrums of the Mg-4Y-xZn alloys, indicating that when the Zn content exceeds 2 wt. %, the content of Mg<sub>24</sub>Y<sub>5</sub> phase decreased until disappeared, while the W phase began to appear and the content gradually increased. In addition to the α-Mg, WZ41 is composed of X phase and Mg<sub>24</sub>Y<sub>5</sub>, both WZ42 and WZ43 are composed of X phase, W phase, and Mg<sub>24</sub>Y<sub>5</sub>, and WZ44 is composed of W phase [24, 25].

Fig. 2 shows the SEM microstructure and EDS results of Mg-4Y-xZn alloys. WZ41 is composed of matrix, lamellar phase, and blocky white granules. WZ42 and WZ43 are composed of matrix, lamellar phase, blocky white granules, and white eutectic network. WZ44 is only composed of matrix and white eutectic network. With the increase of zinc content,



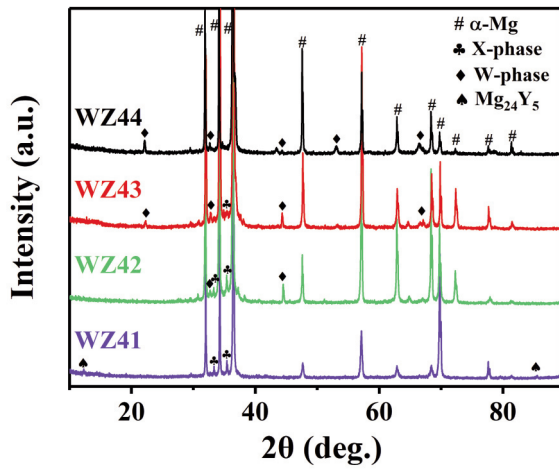


Figure 1. XRD spectrums of as-cast Mg-4Y-xZn alloys

the lamellar phase gradually decreases, while the reticular white eutectic phase gradually increases. Combining the results of XRD, EDS and the detailed analysis in our previous work [12], it can be obtained that the white massive particles corresponding to point A are  $Mg_{24}Y_5$ , the flake phase corresponding to point B is X phase, the white eutectic network corresponding to point C is W phase, and the matrix is  $\alpha$ -Mg. According to Fig. 2(d), W phase in WZ42 appears in the lamellar X phase as a sheet. Fig. 2(f) shows that the W phase in WZ43 appears near the

surface of X phase [26-28].

Fig. 3 is the average corrosion rate of as-cast Mg-4Y-xZn alloys immersed in 3.5 wt.% NaCl solution at 25 °C for 72 h. The results reveal that the corrosion rate increases with the increase of Zn content. Moreover, the corrosion rate of WZ41 is the lowest, and that of WZ44 is the highest. Nevertheless, WZ43 shows lower corrosion rate than WZ42, combine with the microstructure of the alloy, this may be because WZ43 alloy contains more W phase than WZ42 alloy, which affects the corrosion rate.

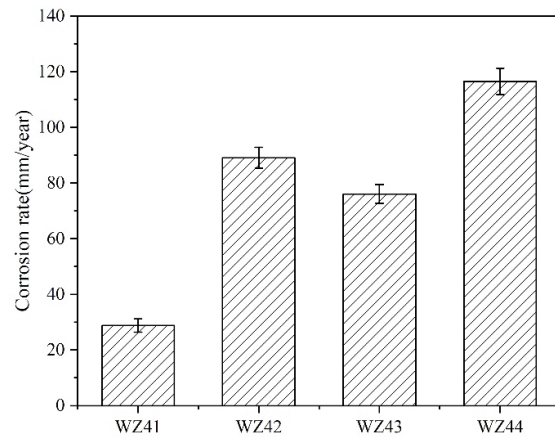


Figure 3. Average corrosion rate calculated from the weight loss after immersion in 3.5 wt. % NaCl solution at 25 °C for 72 h

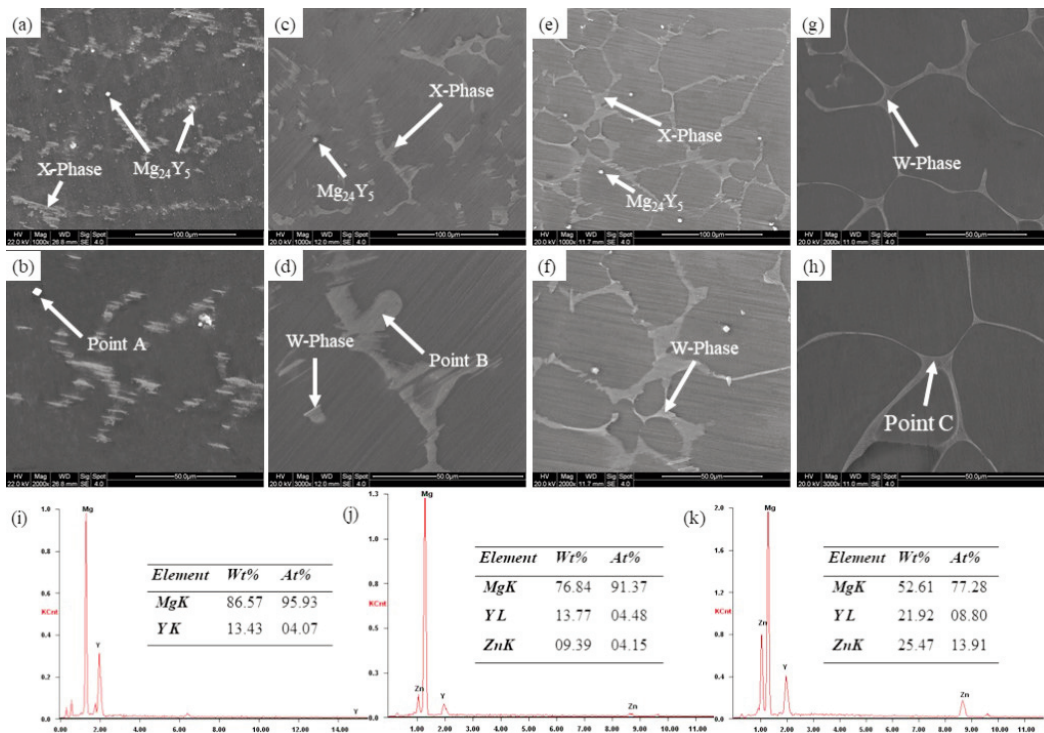
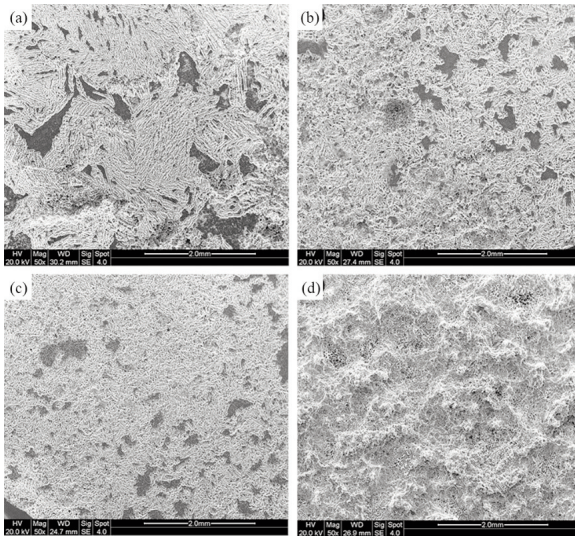


Figure 2. SEM morphologies of as-cast Mg-4Y-xZn alloys: (a) and (b) WZ41, (c) and (d) WZ42, (e) and (f) WZ43, (g) and (h) WZ44, (i) EDS result of point A in (b), (j) EDS result of point B in (d), (k) EDS result of point C in (h)



The corrosion surface of the alloy immersed for 12 h and removed the corrosion products is shown in Fig. 4. Obviously, the corrosion began and gradually



**Figure 4.** Corrosion surface after immersion in 3.5 wt.% NaCl solution for 12 h with removal of corrosion products: (a) WZ41; (b) WZ42; (c) WZ43; (d) WZ44

expanded in the form of pitting corrosion, and a certain number of corrosion pits appeared on the alloy surface. Among them, WZ41, WZ42, and WZ43 alloys showed the characteristics of filamentous corrosion, part of uncorroded substrate still exists in the surface of the above alloys, demonstrating the relatively low corrosion pit expansion rate and weak corrosion occurs. With the increase of Zn content, the characteristics of filamentous corrosion became insignificant [29]. The surface of WZ44 alloy shows

the most serious corrosion behavior. The bare matrix is almost invisible. The surface is composed of corrosion pits with different shapes and sizes.

SEM images shown in Fig. 5 and 6 reveal the corrosion morphology of the alloy after immersion for 5 min, 30 min, 2 h, and 12 h. For WZ41 alloy, the corrosion pits first appear in the vicinity of X phase and  $Mg_{24}Y_5$  phase, while the center of  $\alpha$ -Mg and second phase is basically intact, indicating that the corrosion begins at the junction of  $\alpha$ -Mg and second phase. Then the corrosion pits gradually extended to the  $\alpha$ -Mg, and part of the second phase gradually detach from the surface due to the loss of support from matrix. And then, the second phase is almost completely detached. Finally, it shows that the corrosion pits have begun to expand to the matrix and show the characteristics of filamentous corrosion. For WZ42 and WZ43 alloys, similar to WZ41 alloy, the corrosion pits begin at the junction of the second phase and matrix.

Then the X phase was dissolved or detached, but the W phase was retained; And then, the second phase was completely removed, the corrosion pits began to expand to matrix and left obvious corrosion pits. Finally, the corrosion pits continue to expand and have bare matrix residues, showing the characteristics of filamentous corrosion. For WZ44 alloy, the corrosion pits begin at the junction of W phase and matrix; then, the W phase was gradually eroded and removed leaving a reticular gully. After that, the corrosion pits began to expand to the matrix, leaving only some uncorroded matrix; Finally, the alloy surface is completely occupied by corrosion pits, and there is no exposed matrix. In summary, it can be found that the corrosion pits of the four alloys began at the junction of the second phase and the  $\alpha$ -Mg, and

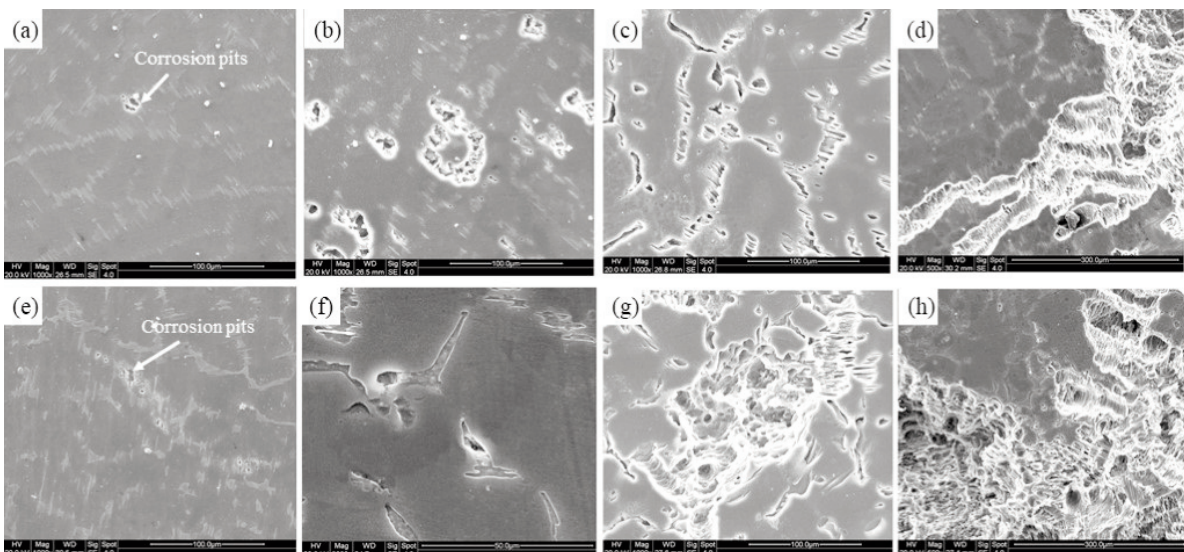


**Figure 5.** Corrosion micrographs of (a-d) WZ41 and (e-h) WZ42 after immersion in 3.5 wt.% NaCl solution for (a, e) 5 min, (b, f) 30 min, (c, g) 2 h, (d, h) 12 h and removal of the corrosion products

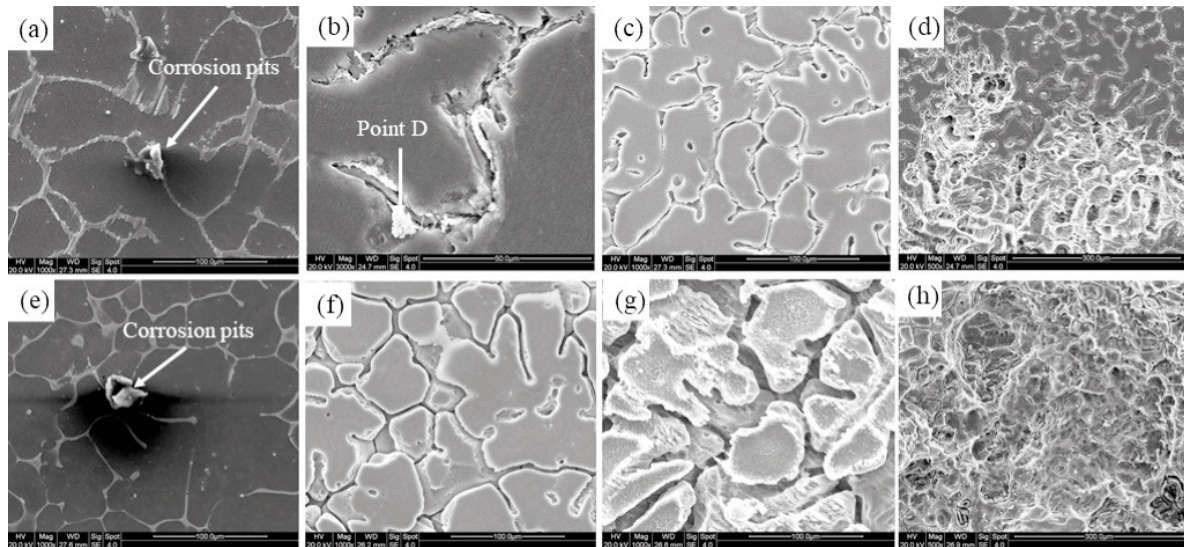


**Figure 6.** Corrosion micrographs of (a-d) WZ43 and (e-h) WZ44 after immersion in 3.5 wt.% NaCl solution for (a, e) 5 min, (b, f) 30 min, (c, g) 2 h, (d, h) 12 h and removal of the corrosion products

then the second phase was gradually eroded or detached, and then began to expand to the matrix, and finally formed obvious corrosion pits. However, for WZ42 and WZ43 alloys, after immersion for 30 min, it can be found that W phase is retained compared with X phase. Considering that the W phase still exists, the possibility of the X phase falling off is not very great, which may be caused by the formation of micro-galvanic cells between X phase and W phase leading to the dissolution of the X phase as an anode. As shown in Fig. 7, the EDS results for point D in Fig. 6 (b) also confirm that the W phase is retained during the initial corrosion process, but a slight corrosion occurs on its surface and is gradually eroded during the subsequent corrosion expansion. As for four alloys, in addition to WZ44 alloy, WZ41, WZ42, and WZ43 alloy eventually showed the characteristics of

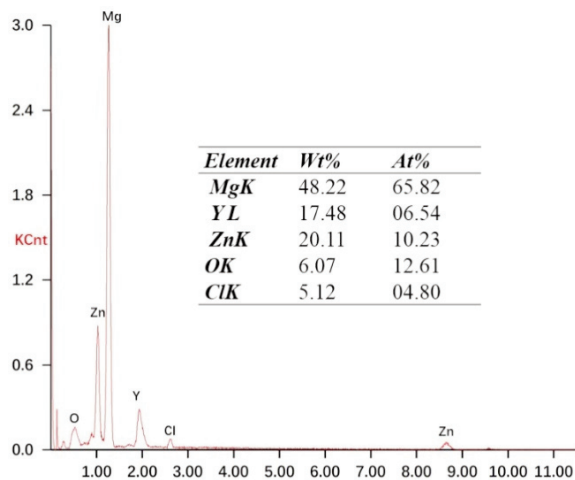


**Figure 7.** EDS result of point D in Fig. 6 (b)

filamentous corrosion. Secondly, the corrosion pit expansion rate of WZ41 alloy is the lowest, and that of WZ44 alloy is the highest, which has been seriously expanded to matrix at 2 h.

Previous studies have shown that the second phase in Mg alloy can present as cathode in the corrosion process to accelerate micro-galvanic corrosion. Siqi Yin et al. revealed that compared with the matrix, W phase and X phase have higher potential, and W phase is electrochemically nobler than X phase [30, 31]. Therefore, the type and the quantity of the second phase have a significant impact on the corrosion process [32, 33]. Obviously, the micro-galvanic corrosion occurs at the junction of the second phase with  $\alpha$ -Mg, which makes the  $\alpha$ -Mg dissolve as an anode. With the extension of soak time, the corrosion pits gradually expanded, and then the second phase eroded or detached to form corrosion ravine. A. Srinivasan et al. also confirmed that sodium chloride solution changed the stability of the W phase at the end of corrosion, and the corrosion products strongly alkalinized the surface after long-term immersion, so that the exposed W phase gradually dissolved and removed [34]. Similar observations were made by Neil et al. in ZE41 alloy [35, 36]. In addition, Ziyou Ding et al. found that during the corrosion process of Mg-Li-Ca alloy, the second phase will occur exfoliation corrosion under the synergistic effect of pitting, filamentous, and intergranular corrosion, and the second phase will fall off from the matrix [37]. Guijia Gao et al. also obtained similar conclusions [38]. As for WZ41 alloys, due to the low content of X phase, the number of micro-galvanic cells formed is limited, which shows the best corrosion performance. As for WZ42 and WZ43 alloys, due to the X phase is



stable in the sodium chloride solution and will not be dissolved, but W phase is electrochemically nobler than X phase. Therefore, micro-galvanic cells will be formed at the junction of X phase and W phase, so that the X phase is used as an anode to dissolve during the corrosion process, thereby reducing the number of micro-galvanic cells formed between the second phase and matrix, whereupon slowing down the corrosion rate of matrix to some extent. Since WZ43 alloy contains more W phase which is located on the surface of X phase, more X-W micro-galvanic cells are formed, so it has better corrosion resistance than WZ42 [38, 39]. The results of the above-mentioned weight loss experiment also verify this result. In addition, in the later stage of corrosion development, some X phase will also fall off from the matrix due to exfoliation corrosion, which is also observed in Fig. 5 and 6. As for WZ44 alloy, due to the higher potential of W phase than  $\alpha$ -Mg, the trend of micro-current corrosion is the largest, showing more obvious corrosion characteristics and the worst corrosion performance. For  $Mg_{24}Y_5$  phase, although micro-galvanic cells can also be formed with  $\alpha$ -Mg, it has little effect on the overall corrosion behavior due to its low content and detached at the end of corrosion.

### 3.2. Electrochemical testing

Fig. 8 shows the polarization curves of Mg-4Y-xZn alloy in 3.5 wt.% NaCl solution, the results fitted by Tafel extrapolation method and listed in Table 1. It is generally believed that the cathode branch is related to the reactive precipitation of hydrogen, while the anode branch is related to the reactive dissolution of matrix. It can be seen that the cathode branch and anode branch in the polarization curve are obviously different, and the increase rate of the curve in the

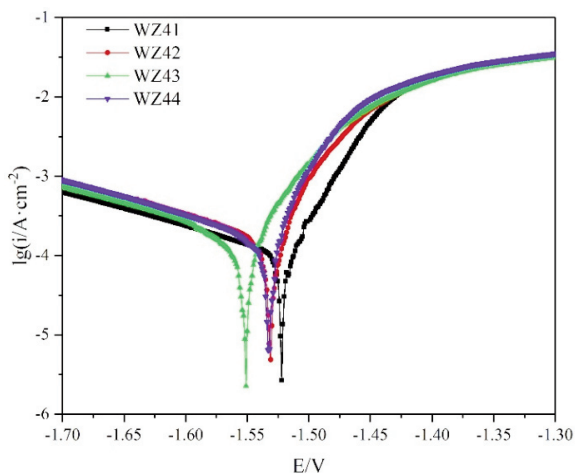


Figure 8. Potentiodynamic polarization curves of WZ41, WZ42, WZ43 and WZ44 alloys measured in 3.5 wt.% NaCl solution

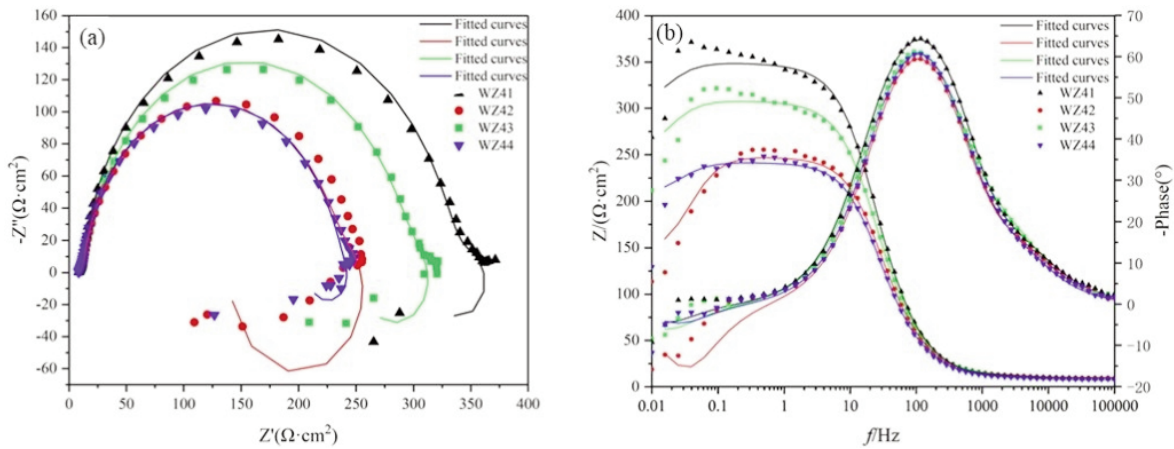
anode branch is much larger than that in the cathode branch [40-42]. In addition, from the cathode point of view, the alloy system has similar polarization behavior and a wide linear Tafel region, which indicates that the alloy has a uniform and stable corrosion rate. As for the anode branch, no obvious passivation phenomenon was found, which reveal that the phase composition of the alloy had little effect on the formation and dissolution of the surface oxide film [34]. According to the fitting results of table 2, the corrosion current density ( $J_{corr}$ ) of the four alloys is  $WZ44 > WZ42 > WZ43 > WZ41$ , and the polarization resistance ( $R_p$ ) increases in turn. It is generally believed that the value of  $J_{corr}$  reflects the actual corrosion rate of the alloy from corrosion kinetics, so WZ41 alloy shows the best corrosion performance. However, WZ43 alloy has the most negative corrosion potential ( $E_{corr}$ ). From the thermodynamic point of view, the corrosion tendency of WZ43 alloy is the highest, but actually it does not show the worst corrosion performance. This also reflects that the actual corrosion rate and mechanism of the alloy are closely related to the microstructure and other factors [30].

Table 2. Electrochemical parameters obtained from polarization curves in Fig. 8

Alloys	$E_{corr}$ /V	$J_{corr}$ / $\mu A \cdot cm^{-2}$	$\beta_a$ /mv·dec <sup>-1</sup>	$\beta_c$ /mv·dec <sup>-1</sup>	$R_p$ / $\Omega$
WZ41	-1.52	130	45.4	-292	131
WZ42	-1.53	231	48.1	-298	77.9
WZ43	-1.55	221	58.8	-308	96.8
WZ44	-1.53	289	55.7	-529	75.8

Fig. 9 shows the EIS curves measured after the 3.5 wt.% NaCl solution was stabilized for 3600 s. In Nyquist plot, the Mg-4Y-xZn alloys show obvious characteristics of high frequency capacitance ring and low frequency inductance ring. Generally, the former can be attributed to the charge transfer process of the double layer and the electrode/electrolyte interface, while the latter can be ascribed to the damage of the surface film and the corrosion nucleation at the incipient stage of local corrosion. Among them, the larger the radius of the high frequency capacitance ring, the larger the charge transfer resistance, which reflects the stability of the surface layer, so that the impedance is significantly improved [41, 42]. With the increase of Zn content, the size of the capacitance ring is roughly reduced, indicating that the corrosion resistance is gradually reduced. However, WZ43 alloy shows a larger capacitance ring than WZ42 alloy, which is also caused by the formation of X-W micro-galvanic mentioned above. In addition, all alloys show certain induction characteristics, among which





**Figure 9.** Electrochemical impedance spectrum (EIS) plots of the alloys: (a) Nyquist plots; (b) Bode phase angle and impedance plots

WZ42 is the most obvious, which means that the surface film of WZ42 alloy is very unstable and has poor protection. The Bode phase angle and impedance plots are shown in Fig. 9(b), as for the Bode plots of phase angle ( $\theta$ ) vs.  $\log f$ , it can be seen that the four alloys are composed of a peak and a trough; usually, a peak represents a time constant. In this case, the peak represents the high-frequency capacitance ring, and the trough represents the low-frequency inductance ring. The large phase angle peak and peak width in the WZ41 alloy demonstrate large resistance and small capacitance, so as to the preferable corrosion protection. As for the Bode plots of  $\log |Z|$  vs.  $\log f$ , in the high frequency region, the impedance values of the four alloys increased significantly, the increase rate slowed down and gradually stabilized in the intermediate frequency range, and the impedance value began to decrease in the low frequency region. Among them, with the increase of Zn content, the variation trend of the impedance modulus of the alloy is similar to that of the capacitance ring size, showing a gradual decrease. The impedance modulus of WZ41 alloy is the largest, which means that it has high polarization resistance. The impedance modulus of

WZ43 alloy is larger than that of WZ42, and the specific reason is the same as that of Nyquist. In addition, it can be seen that the impedance modulus of all alloys decreased significantly in the low frequency region, and the impedance modulus of WZ42 alloy decreased fastest, indicating the instability of its surface film.

To reveal the corrosion mechanism of the alloy, the EIS equivalent circuit model shown in Fig. 10 is provided to fit the corrosion system.  $R_s$  is the solution resistance;  $R_{ct}$  is the charge transfer resistance;  $R_f$  is the membrane resistance. CPE is a constant phase element. Due to the instability of the electrochemical system, the ideal capacitance is replaced by the ideal capacitance to represent the incompleteness of the double layer capacitance. It is defined by two parameters  $Y$  and  $n$ .  $Y$  represents the non-ideal capacitance, which is attributed to the dispersion effect caused by cracks, surface oxide films, impurities, and the second phase;  $n$  is the dispersion coefficient. When  $n = 1$ , CPE is the same as the pure capacitance, and when  $n = 0$ , CPE is the same as the pure resistance. In addition,  $R_{ct}$  and  $CPE_{dl}$  are combined to describe the high-frequency capacitor

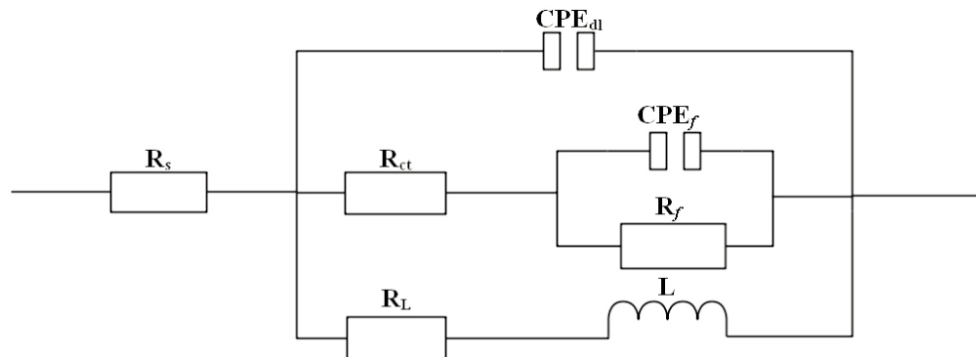


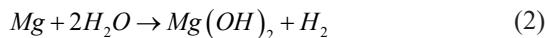
**Figure 10.** Equivalent circuit of the EIS spectra for the alloys immersed in 3.5 wt.% NaCl solution



loop; RL represents the resistance, and L represents the inductance, and together they represent the low-frequency inductance loop, showing the beginning of local corrosion;  $R_f$  and  $CPE_f$  are combined to represent the mass transfer during the dissolution of corrosion products [30, 31].

The EIS curves measured in the experiment were fitted based on the proposed equivalent circuit model, and the fitting results are listed in Table 3. Generally speaking, the higher the values of  $R_{ct}$  and  $R_f$ , the lower the dissolution rate of the matrix, the better the protective performance of the surface film and the better the corrosion resistance. In general, the  $R_{ct}$  and  $R_f$  values of the Mg-4Y-xZn alloys are basically WZ41 > WZ43 > WZ42 > WZ44. However, combined with the previous experimental results, WZ41 alloy should have the maximum  $R_{ct}$  value, but it is actually less than WZ43 alloy. This may stem from the formation of micro-galvanic cells between W phase and X phase in WZ43 alloy, which reduces the corrosion rate of matrix at the initial stage of corrosion [40].

Fig. 11 shows the XRD spectrums of the corrosion products of the Mg-4Y-xZn alloys soaked in 3.5 wt.% NaCl solution at 25 °C for 72 h, which reveals that the corrosion products are consisted of  $Mg(OH)_2$ , with the exception of the WZ44 alloy, the other three alloys also have a small amount of X phase. When the alloy is placed in the NaCl solution, the reaction is shown as follows:



According to the previous results, since the content of W phase gradually increases, during the corrosion stage, the X phase is dissolved as an anode due to the formation of X-W micro-galvanic, so that the peak strength of X phase in the corrosion product of WZ41 alloy is the highest. The  $Mg(OH)_2$  was formed in the whole corrosion process, and a small amount of X phase can be attributed to the exfoliation corrosion occurring at the grain boundaries of X phase

and matrix; subsequently, some small X phases are retained in the corrosion products due to the absence of matrix support. However, the W phase dissolved gradually in the corrosion process, and no W phase was found in the corrosion products.

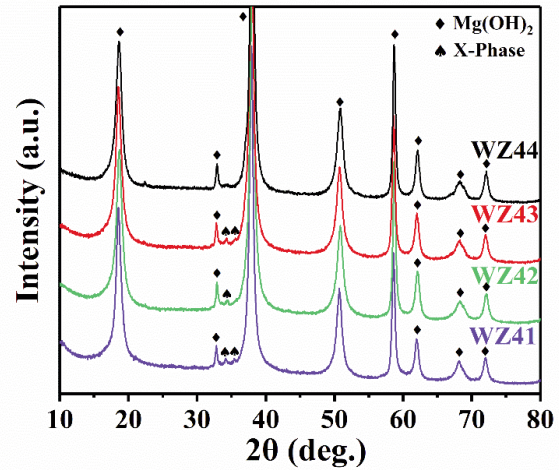


Figure 11. XRD patterns of corrosion product of Mg-4Y-xZn alloys after immersion in 3.5 wt.% NaCl solution for 72 h at 25 °C

#### 4. Conclusions

By studying the microstructure, corrosion behavior and properties of Mg-4Y-xZn alloy with different second phase composition in 3.5 wt.% NaCl solution for different soaking time, the following conclusions can be drawn:

(1) With the increase of Zn content, the main second phase in the Mg-4Y-xZn alloy gradually changed from X phase to X + W phase and finally all became W phase;

(2) The immersion test and electrochemical test confirmed that with the increase of Zn content, the corrosion resistance of Mg-4Y-xZn alloy generally shows a gradual decline, but WZ43 alloy showed better corrosion resistance than WZ42;

Table 3. The fitted EIS data on the basis of the equivalent circuits presented in Fig. 10

Alloys	$R_s$ $\Omega \cdot \text{cm}^2$	$R_{ct}$ $\Omega \cdot \text{cm}^2$	$CPE_{dl}$		$R_L$ $\Omega \cdot \text{cm}^2$	L H	$R_f$ $\Omega \cdot \text{cm}^2$	$CPE_f$	
			$Y_{dl}/\Omega^{-1} \cdot \text{cm}^{-2} \cdot \text{s}^n$	$n_{dl}$				$Y_f/\Omega^{-1} \cdot \text{cm}^{-2} \cdot \text{s}^n$	$n_f$
WZ41	8.602	9.029	$3.172 \times 10^{-5}$	0.867	1945	20980	331.1	$1.119 \times 10^{-5}$	1
WZ42	9.209	6.967	$1.572 \times 10^{-5}$	0.933	308.7	1969	230.9	$2.898 \times 10^{-5}$	0.929
WZ43	9.005	13-dec	$3.051 \times 10^{-5}$	0.882	1231	12490	285.8	$1.588 \times 10^{-5}$	0.96
WZ44	8.411	6.785	$2.219 \times 10^{-5}$	0.925	1282	8567	226	$2.656 \times 10^{-5}$	0.933

(3) The type and content of the second phase play an essential role in the corrosion mechanism and corrosion rate of the alloy. The potential between the  $\alpha$ -Mg and the second phase is different. In the immersion process, the second phase acts as the cathode, and the micro-galvanic corrosion dominates, accelerating the dissolution of the matrix. X phase can be used as an anode in the micro-galvanic cells formed with W phase, which reduced the number of micro-galvanic cells between X phase and  $\alpha$ -Mg, thereby protecting the matrix from corrosion;

(4) The corrosion products of the Mg-Y-Zn alloy consist mainly of  $\text{Mg}(\text{OH})_2$ . Except for the WZ44 alloy, a small amount of X phase is also present in the corrosion products of the remaining alloys.

### Acknowledgments

*This work was supported by the National Key R&D Program of China (2016YFB0301000), Jiangsu Province Scientific and Technological Achievements Transformation Project (BA2016039).*

### Author contributions

*Yong Shi: Performed the experiments, collected the data and wrote the original draft; Xiqin Liu: Provided the financial support for the project and revised the draft; Zili Liu: Writing - review & editing; Huanjian Xie: Analyzed the results and revised the original draft; Yunhao Wang: Data curation; Jian Li: Data curation.*

### Data availability

*The raw/processed data required to reproduce these findings cannot be shared at this time as the data also forms part of an ongoing study.*

### Declaration of competing interest

*The authors declare that they have no known competing financial interests or personal relationships that could have appeared to influence the work reported in this paper.*

### References

- [1] X. J. Wang, D. K. Xu, R. Z. Wu, What is going on in magnesium alloys?, *Journal of Materials Science & Technology*, 34 (2) (2018), 245-247. <https://doi.org/10.1016/j.jmst.2017.07.019>
- [2] T. T. T. Trang, J. H. Zhang, J. H. Kim, Designing a magnesium alloy with high strength and high formability, *Nature Communications*, 9 (1) (2018), 2522. <https://doi.org/10.1038/s41467-018-04981-4>
- [3] F. S. Pan, M. B. Yang, X. H. Chen, A review on casting magnesium alloys: Modification of commercial alloys and development of new alloys, *Journal of Materials Science & Technology*, 32 (12) (2016) 1211-1221. <http://dx.doi.org/10.1016/j.jmst.2016.07.001>
- [4] B. Smola, I. Stulková, F. V. Buch, Structural aspects of high performance Mg alloys design, *Materials Science and Engineering: A*, 324 (1) (2002) 113-117. [https://doi.org/10.1016/S0921-5093\(01\)01291-6](https://doi.org/10.1016/S0921-5093(01)01291-6)
- [5] W. J. Joost, P. E. Krajewski, Towards magnesium alloys for high-volume automotive applications, *Scripta Materialia*, 128 (2017) 107-112. <http://dx.doi.org/10.1016/j.scriptamat.2016.07.035>
- [6] G. Song, A. Atrens, Understanding magnesium corrosion - A framework for improved alloy performance, *Advanced Engineering Materials*, 5 (12) (2003) 837-858. <https://doi.org/10.1002/adem.200310405>
- [7] M. Esmaily, J. E. Svensson, S. Fajardo, Fundamentals and advances in magnesium alloy corrosion, *Progress in Materials Science*, 89 (2017) 92-193. <http://dx.doi.org/10.1016/j.pmatsci.2017.04.011>
- [8] Y. Kawamura, K. Hayashi, A. Inoue, Rapidly solidified powder metallurgy Mg97Zn1Y2 alloys with excellent tensile yield strength above 600 MPa, *Materials Transactions*, 42 (7) (2001) 1172-1176. <https://doi.org/10.2320/matertrans.42.1172>
- [9] T. Itoi, T. Seimiya, Y. Kawamura, Long period stacking structures observed in Mg97Zn1Y2 alloy, *Scripta Materialia*, 51 (2) (2004) 107-111. <https://doi.org/10.1016/j.scriptamat.2004.04.003>
- [10] X. H. Shao, Z. Q. Yang, X. L. Ma, Strengthening and toughening mechanisms in Mg-Zn-Y alloy with a long period stacking ordered structure, *Acta Materialia*, 58 (14) (2010) 4760-4771. <https://doi.org/10.1016/j.actamat.2010.05.012>
- [11] Y. M. Zhu, A. J. Morton, J. F. Nie, The 18R and 14H long-period stacking ordered structures in Mg-Y-Zn alloys, *Acta Materialia*, 58 (8) (2010) 2936-2947. <https://doi.org/10.1016/j.actamat.2010.01.022>
- [12] H. J. Xie, Z. L. Liu, X. Q. Liu, Microstructure, generation of intermetallic compounds and mechanical strengthening mechanism of as-cast Mg-4Y-xZn alloys, *Materials Science and Engineering: A*, 797 (2020) 139948. <https://doi.org/10.1016/j.msea.2020.139948>
- [13] H. J. Xie, Z. L. Liu, X. Q. Liu, Effect of aluminum addition on lattice parameter, formation of intermetallic compounds and mechanical properties of Mg-4Y alloys, *Materials Science and Engineering: A*, 766 (2019) 138359. <https://doi.org/10.1016/j.msea.2019.138359>
- [14] Z. Q. Zhang, X. Liu, W. Y. Hu, Microstructures, mechanical properties and corrosion behaviors of Mg-Y-Zn-Zr alloys with specific Y/Zn mole ratios, *Journal of Alloys and Compounds*, 624 (2015) 116-125. <http://dx.doi.org/10.1016/j.jallcom.2014.10.177>
- [15] C. Q. Li, D. K. Xu, Z. R. Zeng, Effect of volume fraction of LPSO phases on corrosion and mechanical properties of Mg-Zn-Y alloys, *Materials & Design*, 121 (2017) 430-441. <http://dx.doi.org/10.1016/j.matdes.2017.02.078>
- [16] L. Bao, Z. Q. Zhang, Q. C. Le, Corrosion behavior and mechanism of Mg-Y-Zn-Zr alloys with various Y/Zn mole ratios, *Journal of Alloys and Compounds*, 712 (2017) 15-23. <http://dx.doi.org/10.1016/j.jallcom.2017.04.053>



- [17] A. E. Coy, F. Viejo, P. Skeldon, Susceptibility of rare-earth-magnesium alloys to micro-galvanic corrosion, *Corrosion Science*, 52 (12) (2010) 3896-3906. <https://doi.org/10.1016/j.corsci.2010.08.006>
- [18] N. Hara, Y. Kobayashi, D. Kagaya, Formation and breakdown of surface films on magnesium and its alloys in aqueous solutions, *Corrosion Science*, 46 (1) (2007) 166-175. <https://doi.org/10.1016/j.corsci.2006.05.033>
- [19] S. Izumi, M. Yamasaki, Y. Kawamura, Relation between corrosion behavior and microstructure of Mg-Zn-Y alloys prepared by rapid solidification at various cooling rates, *Corrosion Science*, 51 (2) (2009) 395-402. <https://doi.org/10.1016/j.corsci.2008.11.003>
- [20] M. Liu, P. Schmutz, P. J. Uggowitzer, The influence of yttrium (Y) on the corrosion of Mg-Y binary alloys, *Corrosion Science*, 52 (11) (2010) 3687-3701. <https://doi.org/10.1016/j.corsci.2010.07.019>
- [21] Y. W. Song, D.Y. Shan, R. S. Chen, Effect of second phases on the corrosion behaviour of wrought Mg-Zn-Y-Zr alloy, *Corrosion Science*, 52 (5) (2010) 1830-1837. <https://doi.org/10.1016/j.corsci.2010.02.017>
- [22] M. Yamasaki, S. Izumi, Y. Kawamura, Corrosion and passivation behavior of Mg-Zn-Y-Al alloys prepared by cooling rate-controlled solidification, *Applied Surface Science*, 257 (19) (2011) 8258-8267. <https://doi.org/10.1016/j.apsusc.2011.01.046>
- [23] J. Zhu, X. H. Chen, L. Wang, High strength Mg-Zn-Y alloys reinforced synergistically by Mg<sub>12</sub>ZnY phase and Mg<sub>3</sub>Zn<sub>3</sub>Y<sub>2</sub> particle, *Journal of Alloys and Compounds*, 703 (2017) 508-516. <http://dx.doi.org/10.1016/j.jallcom.2017.02.012>
- [24] S. Q. Luo, A. T. Tang, Effect of mole ratio of Y to Zn on phase constituent of Mg-Zn-Zr-Y alloys, *Transactions of Nonferrous Metals Society of China*, 21 (4) (2011) 795-800. [https://doi.org/10.1016/S1003-6326\(11\)60783-8](https://doi.org/10.1016/S1003-6326(11)60783-8)
- [25] Z. Q. Zhang, X. Liu, Z. K. Wang, Effects of phase composition and content on the microstructures and mechanical properties of high strength Mg-Y-Zn-Zr alloys, *Materials & Design*, 88 (2015) 915-923. <http://dx.doi.org/10.1016/j.matdes.2015.09.087>
- [26] Z. H. Huang, S. M. Liang, R. S. Chen, Solidification pathways and constituent phases of Mg-Zn-Y-Zr alloys, *Journal of Alloys and Compounds*, 468 (1-2) (2009) 170-178. <https://doi.org/10.1016/j.jallcom.2008.01.034>
- [27] B. Chen, D. L. Lin, X. Q. Zeng, Effects of yttrium and zinc addition on the microstructure and mechanical properties of Mg-Y-Zn alloys, *Journal of Materials Science*, 45 (9) (2010) 2510-2517. <https://doi.org/10.1007/s10853-010-4223-z>
- [28] J. Gröbner, A. Kozlov, X. Y. Fang, Phase equilibria and transformations in ternary Mg-rich Mg-Y-Zn alloys, *Acta Materialia*, 60 (17) (2012) 5948-5962. <http://dx.doi.org/10.1016/j.actamat.2012.05.035>
- [29] S. D. Wang, D. K. Xu, X. B. Chen, Effect of heat treatment on the corrosion resistance and mechanical properties of an as-forged Mg-Zn-Y-Zr alloy, *Corrosion Science*, 92 (2015) 228-236. <http://dx.doi.org/10.1016/j.corsci.2014.12.008>
- [30] S. Q. Yin, W. C. Duan, W. H. Liu, Influence of specific second phases on corrosion behaviors of Mg-Zn-Gd-Zr alloys, *Corrosion Science*, 166 (2020) 108419. <https://doi.org/10.1016/j.corsci.2019.108419>
- [31] J. Liu, L. X. Yang, C. Y. Zhang, Significantly improved corrosion resistance of Mg-15Gd-2Zn-0.39Zr alloys: Effect of heat-treatment, *Journal of Materials Science & Technology*, 35 (8) (2019) 1644-1654. <https://doi.org/10.1016/j.jmst.2019.03.027>
- [32] J. Liu, L. X. Yang, C. Y. Zhang, Role of the LPSO structure in the improvement of corrosion resistance of Mg-Gd-Zn-Zr alloys, *Journal of Alloys and Compounds*, 782 (2019) 648-658. <https://doi.org/10.1016/j.jallcom.2018.12.233>
- [33] S. Leleu, B. Rives, J. Bour, On the stability of the oxides film formed on a magnesium alloy containing rare-earth elements, *Electrochimica Acta*, 290 (2018) 586-594. <https://doi.org/10.1016/j.electacta.2018.08.093>
- [34] A. Srinivasan, C. Blawert, Y. Huang, Corrosion behavior of Mg-Gd-Zn based alloys in aqueous NaCl solution, *Journal of Magnesium and Alloys*, 2 (2014) 245-256. <https://doi.org/10.1016/j.jma.2014.08.002>
- [35] W. C. Neil, M. Forsyth, P. C. Howlett, Corrosion of magnesium alloy ZE41—The role of microstructural features, *Corrosion Science*, 51 (2009) 387-394. <https://doi.org/10.1016/j.corsci.2008.11.005>
- [36] W. C. Neil, M. Forsyth, P. C. Howlett, Corrosion of heat treated magnesium alloy ZE41, *Corrosion Science*, 53 (2011) 3299-3308. <https://doi.org/10.1016/j.corsci.2011.06.005>
- [37] Z. Y. Ding, L. Y. Cui, R. C. Zeng, Exfoliation corrosion of extruded Mg-Li-Ca alloy, *Journal of Materials Science & Technology*, 34 (2018) 1550-1557. <https://doi.org/10.1016/j.jmst.2018.05.014>
- [38] G. J. Gao, M. Q. Zeng, E. L. Zhang, Dealloying corrosion of anodic and nanometric Mg<sub>41</sub>Nd<sub>5</sub> in solid solution-treated Mg-3Nd-1Li-0.2Zn alloy, *Journal of Materials Science & Technology*, 83 (2021) 161-178. <https://doi.org/10.1016/j.jmst.2020.12.049>
- [39] J. F. Wang, W. Y. Jiang, Y. Ma, Substantial corrosion resistance improvement in heat-treated Mg-Gd-Zn alloys with a long period stacking ordered structure, *Materials Chemistry and Physics*, 203 (2018) 352-361. <https://doi.org/10.1016/j.matchemphys.2017.09.035>
- [40] J. H. Liu, Y. W. Song, J. C. Chen, The special role of anodic second phases in the micro-galvanic corrosion of EW75 Mg alloy, *Electrochimica Acta*, 189 (2016) 190-195. <https://doi.org/10.1016/j.electacta.2015.12.075>
- [41] Z. G. Yang, W. P. Liang, Y. L. Jia, Corrosion behavior of double-glow plasma copperizing coating on Q235 steel, *Journal of Mining and Metallurgy, Section B: Metallurgy*, 56 (2020) 257-268. <https://doi.org/10.2298/JMMB190820017Y>
- [42] L. S. Wang, J. H. Jiang, H. Liu, Microstructure characterization and corrosion behavior of Mg-Y-Zn alloys with different long period stacking ordered structures, *Journal of Magnesium and Alloys*, 8 (2020) 1208. <https://doi.org/10.1016/j.jma.2019.12.009>



## UTICAJ SADRŽAJA Zn NA KOROZIONO PONAŠANJE Mg-Y-Zn LEGURA

Y. Shi <sup>a</sup>, X.-Q. Liu <sup>a,b,\*</sup>, Z.-L. Liu <sup>a,b</sup>, H.-J. Xie <sup>a</sup>, Y.-H. Wang <sup>a</sup>, J. Li <sup>b,c</sup>

<sup>a</sup> Fakultet za nauku o materijalima i tehnologiju, Univerzitet aeronautike i astronautike u Nandžingu, Nandžing, Jiangsu, Kina

<sup>b</sup> Jiangsu (Zhongyi) istraživački centar za precizno livenje pod pritiskom lakih legura, Čangšu, Jiangsu, Kina

<sup>c</sup> Jiangsu Favour Automotive New Stuff Sci-Tech Co., Ltd., Changshu, China

### Apstrakt

Mikrostruktura, koroziono ponašanje i elektrohemijsko ponašanje izlivena Mg-4Y<sub>x</sub>Zn (x=1,2,3,4 wt.%) ispitivano je uz pomoć SEM, gubitka težine, i elektrohemijskih testova. Mg<sub>12</sub>YZn (X), Mg<sub>3</sub>Y<sub>2</sub>Zn<sub>3</sub> (W) i Mg<sub>24</sub>Y<sub>5</sub> čine sistem faznog sastava legure. Kada je sadržaj Zn 1 wt.%, svi testovi pokazuju da legura ima optimalne performanse što se tiče korozije. Druga faza u ovim legurama, budući da je plemenitija od α-Mg, postoji kao katoda tokom procesa korozije, tako da α-Mg prvenstveno izaziva koroziju da bi ubrzao formiranje jamičaste korozije. Posle potapanja u 3.5 wt.% NaCl rastvora na neko vreme, stabilnost W faze se promenila, postepeno se rastvorila, i konačno je odstranjena hromnom kiselinom koja se koristi za uklanjanje proizvoda korozije. Uz to, X faza može da se koristi kao anoda u mikro-galvanskim ćelijama formiranim unutar W faze da bi se redukovala stopa korozije α-Mg i tako poboljšala otpornost na koroziju legure.

**Ključne reči:** Mg-Y-Zn; Druga faza; Korozijsko ponašanje; Elektrohemijsko ponašanje

